Online Parameter Adaptation for the Dynamical Model of a Tri-electrode Zinc-Air Flow Cell

Juan Diego Pineda Rodriguez, Cristina Vlad, Pedro Rodriguez-Ayerbe, Woranunt Lao-Atiman, Sorin Olaru, Soorathep Kheawhom

Online Parameter Adaptation for the Dynamical Model of a Tri-electrode Zinc-Air Flow Cell

Juan Diego Pineda-Rodriguez[1], Cristina Vlad[1], Pedro Rodriguez-Ayerbe[1]
Woranunt Lao-atiman[2], Sorin Olaru[1] and Soorathep Kheawhom[2]

***Abstract*—The paper explores the modeling, prediction, and monitoring of a tri-electrode zinc-air flow cell, contributing to the Battery Management System solutions for zinc-based storage systems. It focuses on airflow batteries, known for their promising safety and robustness features yet exhibiting significant performance variability and parameter fluctuations over cycles and lifespan. Building upon earlier work on modeling and parameter identification at constant current discharge rates and investigations into dynamic behavior changes at varying discharge currents, this study proposes an online parameter adaptation approach based on the structural properties of the dynamical model. This approach uses operational data to mitigate parameter discrepancies arising from zinc reaction chemistry while addressing capacity and current-voltage nonlinearities induced by cell stress from specific discharge profiles.**

I. Introduction

Recently, there has been a significant increase in the research interest regarding energy storage systems [1]. Lithium-ion batteries have dominated the market due to their high energy density, relatively low weight, and long cycle life. However, research is conducted to enhance these solutions [2] and further seek alternatives for the forthcoming limitation on raw materials. This includes increasing energy density, improving safety, reducing charging times, and lowering costs [3]. Moreover, advancements in Battery Management Systems (BMS) and smart grid technologies are optimising the integration of batteries into existing energy infrastructure, enabling more efficient and reliable energy storage solutions [4]. Alternative chemistries like zinc and flow batteries are gaining interest beyond lithium-ion. Flow batteries are suitable for grid-scale energy storage due to their scalability and flexibility. Zinc, one of the most abundant elements, is cost-effective and environmentally friendly for battery production. Being widely available it ensures a stable and sustainable supply chain for battery manufacturing. Safety is paramount when it comes to energy storage, and Zn-based batteries excel in this regard [5]. They are inherently safer than other battery chemistries, with a lower risk of thermal runaway and fire hazards [6]. Furthermore, one of the key metrics for battery performance evaluation is cycle life and Zn-based batteries have proven excellent cycle life [7], making them a durable, long-lasting solution for a variety of applications [8]. While all these advantages are relatively well established, the maturity of zinc-based batteries is far from that of lithium-based technologies. The research community has lately focused on the materials [9] that can advance battery technology, increasing their performance, and accelerate their use across various sectors and applications; a major step forward can be obtained by integrating performant operation within a standardized BMS [10]. Model-based design is essential for understanding and optimizing battery performance. The work to develop comprehensive mathematical models for zinc-air batteries is in its early stages. Several studies have looked into different aspects of these batteries, such as their electrochemical properties [11], their behavior under various discharge rates, especially constant current [12], and responses during dynamic operation [13]. The present paper aims to take a step forward and exploit the structural properties of the existing models (depleting-related nonlinearity, voltage-current static characteristic, and time constants during the transitory) in a real-time framework. The key feature is the adaptation of the model parameters according to the evolution of the cell discharge profile. After recalling the main functional characteristics and modeling principles in Section II, Section III presents a qualitative parameter analysis based on the existing studies in the literature. As a result of this analysis, a strategy for parameter adaptation is elaborated in Section IV as the main contribution. The technical routines exploited for the implementation are based on classical regression and moving horizon estimation procedures, thus offering a robust and flexible real-time monitoring and prediction block for a zinc-air flow cell. Section V offers a detailed analysis of the results and a discussion of the prediction capabilities of the identified model, addressing the challenges and limitations of the proposed online parameter adaptation procedure.

II. Model Structure

A. Principles of operation

The electrochemical phenomenon exploited in this study is an oxidation-reduction reaction between zinc and oxygen. During the discharging cycle of the cell, zinc, acting as the negative electrode (anode), gets oxidated and releases electrons to a potassium hydroxide electrolyte medium that facilitates electron exchange. The intermediate product of this reaction is zincate, which becomes zinc oxide at the end of the reaction. In this process, oxygen is the positive electrode (cathode). Inversely, when charging the cell, zinc oxide inside the electrolyte gets reduced, and oxygen is liberated. As a result, zinc deposits inside the cell which allows for future

*This work was supported by the mobility grants of the STIC Doctoral School of Université Paris-Saclay.

[1]Laboratory of Signals and Systems, Université Paris-Saclay, CNRS, CentraleSupélec, 91190 Gif-sur-Yvette, France {diego.pineda; cristina.vlad; pedro.rodriguez; sorin.olaru}@centralesupelec.fr

[2]Department of Chemical Engineering, Faculty of Engineering, Chulalongkorn University, Bangkok 10330, Thailand, {woranunt.l; soorathep.k}@chula.ac.th

discharge. The chemical reactions are detailed in [13] and the global reaction can be summarized as:

$$\text{Zn} + \frac{1}{2}\text{O}_2 \longleftrightarrow \text{ZnO with } E^0_{\text{cell}} = 1.65V.$$

The theoretical open-circuit voltage is 1.65 V. However, the practical potential distributes around 1.4 V, a consequence of losses caused by the physical construction of the cell and the purity of the air and the electrolyte. A schema of the cell used in this study is presented in Fig. 1, developed in the chemical engineering laboratory at Chulalongkorn University in Bangkok, Thailand. The term *flow* comes from the fact that the electrolyte flows through the cylinder, enhancing the cell's performance as it avoids phenomena such as dendrite formation, passivation, and coalescence [11], [14], [15].

B. Modeling and identification

The zinc-air flow cell encompasses electrochemical and physical interactions that affect its performance and voltage characteristics. Multiple battery modeling techniques can be used depending on available data and tools and the precision required for an application. This study aims to characterize the output voltage behavior of the cell to any given load during its discharge, which the chemical reaction alone fails to provide; therefore, the modeling technique chosen for obtaining the macroscopic behavior of the cell's voltage consists of a grey-box approach written as an input-output block diagram, as shown in Fig. 2. This diagram consists of two main elements:

- A static nonlinear function $f(Z, i)$ that describes the cell's voltage response with respect to two fundamental variables: the applied load (i.e., the current drawn from the cell, i, in amps [A]) and the **discharged capacity** Z, obtained by integrating the current (coulomb counting) and given in amp-hour [mAh]. Both variables, the system's inputs, determine the cell's operating voltage and the voltage drop-point, which indicates the cell's depletion and end of the discharge period. A sigmoidal function can explain the overall discharge stage, with its inflection point marking the end of the discharge and its amplitude varying as a function of the current.
- A first-order differential equation $g(i, V_s)$ that represents the system's transient response when changing the current reference level. This block's input is the steady-state voltage V_s given by function $f(Z, i)$, and its related time constant τ is current-dependent.

The system has several sources of variability that can drive the cell's voltage response away from its nominal characteristics. These disturbances can be put into two variables:

- Immediate variations, such as temperature, electrolyte concentration, and zinc distribution inside the tube, are included in a parameter vector θ_j. It is assumed to be constant along one discharge stage, only changing after the cell is recharged and a new discharge period starts. These variations also affect variables such as the cell's open-circuit voltage and transitory time constants.
- Variations over the cell's lifetime are included in an aging parameter σ, which incorporates the cell's material degradation over time. This parameter is not considered in this study, as the tests were performed consecutively and were not numerous enough to have a noticeable change in the cell's performances. Its impact can be studied in a future analysis of the cell's State-of-Health (SoH).

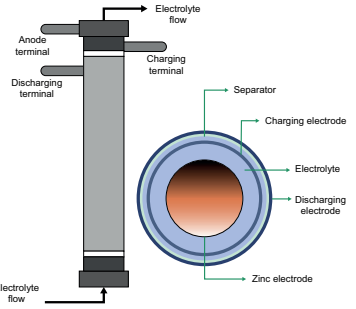

Fig. 1. Description of a tri-electrode rechargeable zinc-airflow cell [16].

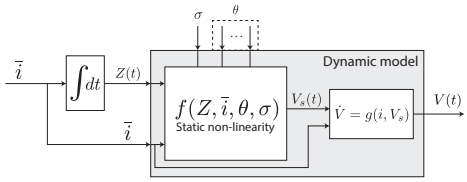

Fig. 2. Proposed block diagram for the modeling based on the extensive analysis of post-operation data [17].

The system dynamics defined in Fig. 2 can be translated into an equivalent first-order RC circuit model, represented in Fig. 3. The circuit's source is the cell's open-circuit voltage V_{OC}, in series with a resistor $R_n(i)$ and a capacitor $C_n(i)$, both current dependent. The voltage on the cell's terminals V, corresponds to the voltage on the capacitor. The current-varying values of the resistor and capacitor incorporate the nonlinear characteristics of the function f, while the RC pair describes the transient behavior of the cell.

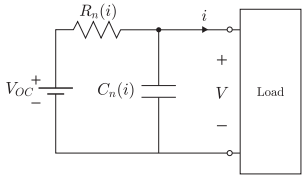

Fig. 3. Equivalent RC circuit.

The equivalent RC circuit dynamic model is written as :

$$\dot{V}(t) = -\frac{1}{\tau}V(t) + \frac{1}{\tau}V_{OC}(t) - \frac{1}{C_n}i(t) \tag{1}$$

with $\tau = R_n C_n$, the current-dependent time constant, and R_n and C_n, values corresponding to the amplitude of a particular discharge current step i_n. Even if the cell remains unchanged, the main challenge regarding the modeling and predictability of its performances is the variability from its construction and environment, which deviates the performances from the expected behavior. This variability does not reflect only on

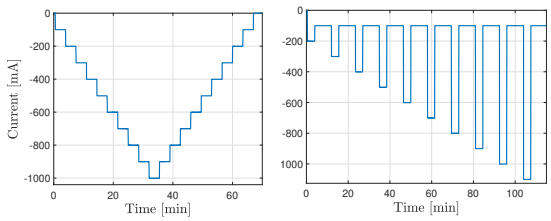

(a) (b)

Fig. 4. Discharge current profiles **a.** 100 mA steps of 3.5 min **b.** Sawtooth profile with a 100 mA offset.

the cell's open-circuit voltage and transitory behavior but also directly on the available capacity, as the point of cell depletion changes from one test to another. This means that the cell's efficiency is not constant. Likewise, the cell's SoH can affect its point of depletion (and therefore its efficiency). With this in mind, the objective of this study is to use the model proposed in Fig. 2 and Eq. (1) to predict the cell's output voltage to different load currents while adapting the model's parameters during the discharge period to account for discrepancies between the model's output and the measured voltage, coming from changes in the parameter vector θ_j.

C. Data collection

Data was collected using a BTS-4000 battery tester from Neware Technologies, which consists of an 8-channel device coupled to a server. After charging the cell with a constant current up to a defined charge $\mathbf{Z_T}$ [mAh], the device was programmed to perform constant-current discharge of the cell to levels of current ranging from 0 to $\approx$ 1 A in steps with variable duration and amplitude, defined by the profiles in Fig. 4 (a negative current indicates discharge). For the sawtooth profiles, the offset current was varied in steps of 100 mA, with the sawtooth current steps varying around that offset. The reference current and output voltage were measured with a sampling time T_s of 100 ms. These profiles were repeated in sequence until the cell's voltage considerably dropped (usually below 0.5 V), which meant the cell's depletion was reached. After depletion, the cell was recharged to prepare for another discharge cycle. At the beginning of every discharge, a 30-second *rest* period was introduced to measure the open-circuit voltage V_{OC}, considered constant for a particular discharge. Since the data collection is innately discrete, Eq. (1) becomes:

$$V[k] = \frac{\tau}{\tau + T_s} V[k-1] + \frac{T_s}{\tau + T_s} V_{OC} - \frac{\tau T_s}{C_n(\tau + T_s)} i[k]. \quad (2)$$

The interest of using this kind of discharge profile is that it delivers a rich amount of data containing the operating voltage of the cell subject to multiple discharge currents within one discharge period, along with the transient responses, which allows limiting the effect of the parameter vector θ_j that would become non-negligible if multiple charge-discharge cycles are performed to test every current.

III. Qualitative Parameter Analysis

The system can be examined from two distinct time scales; the first one said *fast* response, which encompasses the system's transient response with its corresponding time constant, and the steady-state operating voltage for a given load current. The second time scale, said *slow* response, covers the cell's behavior along its entire discharge period, where a sigmoid function explains the output voltage and the integral of the current (i.e., the cell's discharged capacity) comes into play.

A. Fast system variations

Unlike other battery chemistries, such as Li-ion, zinc-air flow batteries have a higher voltage variability when subjected to different discharge rates, as shown in Fig. 5. To better comprehend how the cell's operating voltage evolves depending on the applied load, it is written as a function that associates the open-circuit voltage V_{OC} and a current-dependent voltage $\Delta V(i)$, based on the proposed circuit in Fig. 3:

$$V(i) = V_{OC} - \Delta V(i). \quad (3)$$

The measured discharge curves reveal that ΔV is only a function of the load current i_n *if* the cell's inflection point is still further from the operation point, as seen in Fig. 5 in the *linear region*. By the end of the discharge, ΔV deviates from its tendency owing to the sigmoid's influence on the voltage profile. This phenomenon is observed in Fig. 6a., where a linear function can approximate ΔV for load currents over 200 mA, only deviating upwards when approaching depletion. Similarly, the time constants τ are current-dependent for low currents but remain relatively constant for discharge rate changes in the *linear region*. However, as the end of discharge approaches, the time constant values deviate from their general tendency. Fig. 6b. shows the general behavior of the time constants. The pyramid cycle discharge current profile has shown to help identify an appropriate model by sampling the operating voltage and the transitory behavior of the cell for multiple discharge currents. However, attention has to be given if the objective is to maximize the amount of charge that can be withdrawn from the cell, as higher discharge rates stress the cell and reduce its available capacity.

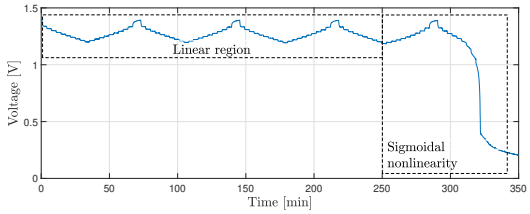

Fig. 5. Complete output voltage profile when repeating the discharge current profile from Fig. 4a until reaching cell's depletion.

B. Slow system variation

When the cell has been discharged for sufficient time, it reaches depletion and the output voltage drops with a sigmoidal shape. The inflection point of the sigmoid (the point of maximum slope) depends on the discharged capacity and the discharge rate, meaning that a higher current will deplete the cell faster. This influences the cell's effective capacity, as higher load currents will drive it away from its nominal capacity. To include the effect of the sigmoid in Eq. (3), it can be stated that the voltage source V_{OC} from the

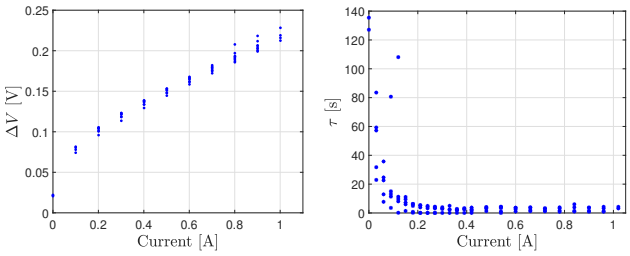

(a) (b)

Fig. 6. a. Operating voltage ΔV and b. τ values as a function of the current.

electric circuit model suffers a sigmoidal drop when subject to a load, given by a function $\Theta(Z)$ of the form:

$$\Theta(Z) = \frac{1}{1 + \mathrm{e}^{m(Z-\eta Z_T)}} \tag{4}$$

where m is the sigmoid's slope at the inflection point, Z is the discharged capacity, Z_T is the *total charged* capacity, and η is a current-dependent coefficient that determines the inflection point of the sigmoid function. It can be assimilated to an efficiency coefficient ranging from 0 to 1. This voltage drop can be seen as a nonlinearity taking effect by the end of the discharge period. Eq. (3) can be rewritten as:

$$V(Z, i) = \Theta(Z)V_{OC} - \Delta V(i). \tag{5}$$

To summarize, the online adapting procedure proposed during the discharge period should take into account the following model's parameters:

- Configuration parameters: V_{OC} parameter is measured during the *rest* period at the beginning of the discharge cycle and assumed constant during the cell's operation.
- Steady-state parameters: ΔV parameter is adapted continuously during the cell's operation.
- Transitory constant: τ is identified using data from the beginning of the *linear region* under a window of size N. The identified value is fixed over the discharge cycle.
- Long-term nonlinearity: parameters m, η of the capacity dependent function $\Theta(Z)$ are assumed to be constant.

IV. Real-time adaptation techniques

Based on the model proposed with the electrical circuit and the block diagram, multiple techniques can be used to identify the model parameters using measured data during the cell's operation.

A. Linear least-squares approach The output of the discrete-time linear model from Eq. (2) is rewritten with the parameters χ_1, χ_2 and χ_3 :

$$V_m[k] = \chi_1 V_m[k-1] - \chi_2 i[k] + \chi_3 V_{OC} \tag{6}$$

where $\chi_1 = \frac{\tau}{\tau+T_s}, \chi_2 = \frac{\tau T_s}{C_n(\tau+T_s)}$ and $\chi_3 = \frac{T_s}{\tau+T_s}$. The error at time k, $\varepsilon[k, \chi]$, is defined as the difference between the observed voltage $V[k]$ and the value predicted by the model $V_m[k]$ while replacing the previous voltage values by observations. The ordinary least squares criterion is the following:

$$J(\chi) = \sum_{k=1}^{N} \varepsilon[k, \chi]^2 = ||\mathcal{E}|| \tag{7}$$

with $\chi = \begin{bmatrix}\chi_1 & \chi_2 & \chi_3\end{bmatrix}^T$. $\mathcal{E}$ is the vector of residuals over the observation window of length N. The parameter vector minimizing the criterion, $\hat{\chi} = \arg\min_\chi J(\chi)$, is computed with the analytical solution:

$$\hat{\chi} = (\mathbf{X}_\chi^T \mathbf{X}_\chi)^{-1} \mathbf{X}_\chi^T \mathbf{Y}_\chi \tag{8}$$

where $\mathbf{X}_\chi \in \mathbb{R}^{N\text{x}3}$ and $\mathbf{Y}_\chi \in \mathbb{R}^{N\text{x}1}$ are composed as:

$$\mathbf{X}_\chi = \begin{bmatrix} V[0] & -i[1] & V_{OC} \\ \vdots & \vdots & \vdots \\ V[N-1] & -i[N] & V_{OC} \end{bmatrix}, \mathbf{Y}_\chi = \begin{bmatrix} V[1] \\ \vdots \\ V[N] \end{bmatrix}. \tag{9}$$

The observation window for the output voltage is selected long enough to capture all current step amplitudes and the steady-state voltages. Two ways of obtaining χ are used:

- Static window at the beginning of every discharge cycle, with $k \in \{1, \ldots, N\}$. k starts counting after the initial *rest* period. χ calculation is performed after storing N samples. This allows a unique calculation that saves resources and memory while adapting the model to the conditions of a particular discharge.
- A moving horizon capturing past outputs and updating the estimation parameter vector, with $k \in \{j - N + 1, \ldots, j\}$, where j marks the current time step. The window is shifted when a fixed number of new samples is received, which prevents reiterating the computations for every sample, making the process computationally expensive. The moving window enables the model's adjustment to consider intrinsic or extrinsic variations in the cell.

For both approaches above, it is necessary to include the sigmoidal nonlinearity in order to capture the long-term information related to the degradation profile of the cell and the time it takes to reach depletion. To accommodate this nonlinearity, V_{OC} is adjusted by a dynamically evolving parameter $\Theta[k]V_{OC}$ in equation (6). In this study, the sigmoid's parameters are constant, with $m = 2.8\text{x}10^{-2}$ and $\eta = 0.97$; however, they can also be adapted in real-time to account for discrepancies between the model and the real system's operation (not within the scope of the present paper).

B. Nonlinear least-squares: This estimation method is also implemented to gain more insight into the cell's behavior. For this approach, the steady-state expression from Eq. (5) is used in the objective function with the current-dependent voltage $\Delta V(i)$ of the form:

$$\Delta V(i) = a + bi[k] - c\mathrm{e}^{-di[k]} \tag{10}$$

so that

$$\hat{\chi} = \arg\min_{\chi} \sum_{k=M+1}^{M+N} (V[k] - V_m[k, \chi])^2 \tag{11}$$

where $V[k]$ is the measured voltage, $V_m[k, \chi]$ corresponds to the output voltage predicted by equations (5) and (10), and $\chi = [a, b, c, d]$ is the parameter vector. Similarly to the linear least-squares, χ is identified using both techniques: one static window at the beginning of the discharge and a moving window. Regarding the time constants τ characterizing the transient behavior, they are current-dependent with the form:

$$\tau(i) = g + h\mathrm{e}^{\rho i}. \tag{12}$$

In this study, parameters g, h, and ρ are identified at the beginning of the discharge.

V. Results

A. Prediction performance

Multiple load current profiles were applied on the cell, as portrayed in Fig. 4, with different step lengths, amplitudes, and offsets. The size N of the windows was modified depending on the test so that the data captured contained sufficiently rich current levels. It should be mentioned that all input profiles were known before starting each test.

1) Static initialization window: The estimation parameter vector $\hat{\chi}$ values were calculated at the beginning of every discharge, with the corresponding window N. This window covers all the output voltages for increasing currents (i.e., the first half of the pyramid for pyramidal profiles). The evolution of $\hat{\chi}$ for 23 discharges is shown in Fig. 7. The evolution of the estimated parameters shows that it is important to recalculate the parameter vector for every discharge, as environmental changes coming from the test setting and unmodelled electrochemical phenomena can impact the cell output voltage. The root-mean-squared error for each test is presented in Fig. 9. The predicted output with a static window for one of the discharges is shown in Fig. 8. It can be observed that the prediction deviates from the real output towards the end of the discharge, which points the study toward the next step: a moving prediction window to adapt the parameter vector.

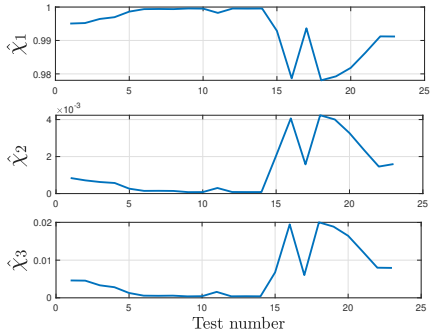

Fig. 7. Evolution of the estimation vector with a static window.

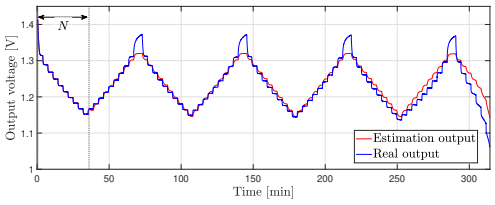

Fig. 8. Real voltage vs estimated output voltage with a static window.

2) Moving horizon parameter estimation: To improve the output voltage prediction, the window N is shifted in a fixed number of p samples whenever they are available, p usually being the length of a single step current. This shift permits to update the estimation parameter vector with the new data. However, the vector $\hat{\chi}$ is sensitive to the size of the window and the type of data contained, which negatively affects the quality of the prediction in two cases:

- The data encompasses falling and rising steps (e.g., in Fig. 8, a bigger window containing the complete pyramid instead of half of it degraded the estimation quality).
- The data encloses rest periods ($i = 0$) or low-current discharges. This results from the nonlinear behavior of the voltage for currents lower than 200 mA (Fig. 6a).

To mitigate these issues, the estimation vector computation was split; $\hat{\chi}_1$ and $\hat{\chi}_3$, were only updated N samples after every rest period and not at every p samples. This limited the number of times both parameters were recalculated and eliminated the effect of zero currents in the estimation. On the other hand, every p samples, $\hat{\chi}_2$ was updated while the other two elements of $\hat{\chi}$ were held constant. This is since $\hat{\chi}$ depends on C_n, which in turn depends on the current. Hence, χ_2 is written as:

$$\chi_2 = \beta_1 + \beta_2 i[k]. \tag{13}$$

The two components $\hat{\beta}_1$ and $\hat{\beta}_2$ were calculated using the least square solution of the same form as equation (8), where $\mathbf{X}_\beta \in \mathbb{R}^{N\text{x}2}$ and $\mathbf{Y}_\beta \in \mathbb{R}^{N\text{x}1}$ are composed as:

$$\mathbf{X}_\beta = \begin{bmatrix} -i[1] & -i^2[1] \\ \vdots & \vdots \\ -i[N] & -i^2[N] \end{bmatrix}, \mathbf{Y}_\beta = \begin{bmatrix} V[1] - \hat{\chi}_1 V[0] - \hat{\chi}_3 V_{OC} \\ \vdots \\ V[N] - \hat{\chi}_1 V[N-1] - \hat{\chi}_3 V_{OC} \end{bmatrix} \tag{14}$$

With a moving estimation window, the $\hat{\chi}$ and $\hat{\beta}$ values change to improve the estimation output as the window moves further following the cell's discharge. The interest in adapting the estimation parameters becomes clearer in Fig. 9, which shows the RMSEs of the non-adapted parameters vs. the minimum RMSEs of the moving horizon. Tests 14 to 16 contained low current discharges and multiple rest periods.

Going further into the analysis, the nonlinear least squares model provides an opportunity to improve the quality of the estimation. The first results regarding the RMSEs are promising. Fig. 10 shows an improved output estimation, mostly on the time constants of the transitory. Fig. 11 shows that while there is a gain in the estimation error on around 60% of the output prediction tests, there is still an improvement to be done, which can be tackled from the size of the horizon, from unchanged variables such as time constants τ or the sigmoid slope and inflection point, or even from an adaptation of the open-circuit voltage V_{OC}.

B. Major challenges and applications

The estimation methods proposed in this study come with some main challenges that cannot be overlooked:

- While a discharge test containing multiple currents may be useful for parameters estimation, this process puts the cell under too much effort, reducing its available capacity.
- The time constants for low currents are larger and must be correctly identified as they can bias the estimation, especially for the nonlinear least squares method.
- Since the cell is not industrially produced, variability between cells increases and requires continuous testing.

- Regarding the previous point, cell testing requires long discharge periods, which limits the available data to be fed to a machine learning algorithm, for example.
- The estimation quality is sensible to the window size N. Depending on the application, memory limitations and computing power can influence the choice of the window size and the estimation method.

Once a model provides sufficient estimation precision, it can be included in a BMS that holds the following tasks:

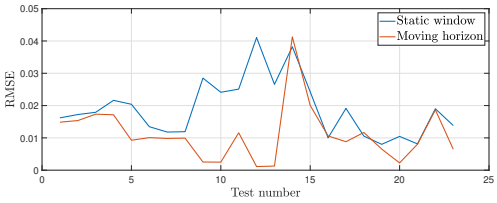

Fig. 9. Static window vs moving window minimum RMSEs.

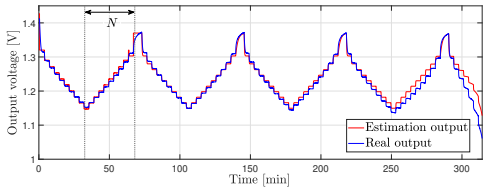

Fig. 10. Output voltage estimated with the nonlinear least squares method.

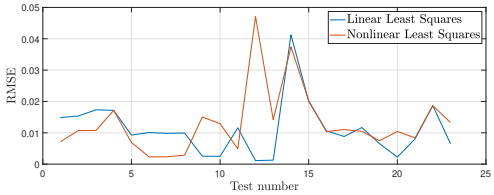

Fig. 11. RMSE comparison for linear and nonlinear least squares methods.

- Safety shutdowns when overloading a cell or battery packs, indicating whenever a current is too high to ensure safe operation and protect the cells.
- Recharge indications when the cell or battery pack nears depletion, based on the output voltage and estimations.
- Profile adapting for extending the battery's discharge duration. Based on desired use and priority tasks, the loads supplied by the battery can be connected or disconnected using an estimated voltage response and predicted depletion. In this study, the current profiles are set beforehand but can be adapted depending on the desired use.
- Cell balancing within battery packs to optimize their global available charge.

VI. Conclusion

The paper presents, to the best of the authors' knowledge, the first attempt to use an online adaptation of dynamic parameters along the operation of a zinc-air flow cell. The study points to the qualitative analysis of the evolution of the open-circuit voltage, the current-voltage static gain or the transitory time constants. It is shown that the parameter identification can be adjusted to exploit the available information by concentrating the computational effort on the meaningful parameters at each phase of functioning.

References

[1] M. M. Rahman, A. O. Oni, E. Gemechu, and A. Kumar, "Assessment of energy storage technologies: A review," *Energy Conversion and Management*, vol. 223, p. 113295, 2020.

[2] K. S. Mawonou, A. Eddahech, D. Dumur, D. Beauvois, and E. Godoy, "State-of-health estimators coupled to a random forest approach for lithium-ion battery aging factor ranking," *Journal of Power Sources*, vol. 484, p. 229154, 2021.

[3] S. J. Moura, F. B. Argomedo, R. Klein, A. Mirtabatabaei, and M. Krstic, "Battery state estimation for a single particle model with electrolyte dynamics," *IEEE Transactions on Control Systems Technology*, vol. 25, no. 2, pp. 453–468, 2016.

[4] V. Casagrande, I. Prodan, S. K. Spurgeon, and F. Boem, "Resilient distributed mpc algorithm for microgrid energy management under uncertainties," in *2022 European Control Conference (ECC)*. IEEE, 2022, pp. 602–607.

[5] J. Fu, Z. P. Cano, M. G. Park, A. Yu, M. Fowler, and Z. Chen, "Electrically rechargeable zinc–air batteries: progress, challenges, and perspectives," *Advanced materials*, vol. 29, no. 7, p. 1604685, 2017.

[6] M. A. Alemu, M. Z. Getie, and A. K. Worku, "Advancement of electrically rechargeable multivalent metal-air batteries for future mobility," *Ionics*, vol. 29, no. 9, pp. 3421–3435, 2023.

[7] P. Pei, K. Wang, and Z. Ma, "Technologies for extending zinc–air battery's cyclelife: A review," *Applied Energy*, vol. 128, pp. 315–324, 2014.

[8] R. Khezri, A. Parnianifard, S. R. Motlagh, M. Etesami, W. Lao-Atiman, A. Abbasi, A. Arpornwichanop, A. A. Mohamad, S. Olaru, and S. Kheawhom, "Performance enhancement through parameter optimization for a rechargeable zinc-air flow battery," *Journal of Industrial and Engineering Chemistry*, vol. 115, pp. 570–582, 2022.

[9] X. Liu, X. Fan, B. Liu, J. Ding, Y. Deng, X. Han, C. Zhong, and W. Hu, "Mapping the design of electrolyte materials for electrically rechargeable zinc–air batteries," *Advanced Materials*, vol. 33, no. 31, p. 2006461, 2021.

[10] A. Löchte *et al.*, "Battery management of rechargeable zinc-air batteries," 2021.

[11] W. Lao-Atiman, K. Bumroongsil, A. Arpornwichanop, P. Bumroongsakulsawat, S. Olaru, and S. Kheawhom, "Model-based analysis of an integrated zinc-air flow battery/zinc electrolyzer system," *Frontiers in Energy Research*, vol. 7, p. 15, 2019.

[12] S. Olaru, A. Golovkina, W. Lao-atiman, and S. Kheawhom, "A mathematical model for dynamic operation of zinc-air battery cells," *IFAC-PapersOnLine*, vol. 52, no. 17, pp. 66–71, 2019.

[13] W. Lao-Atiman, S. Olaru, S. Diop, S. Skogestad, A. Arpornwichanop, R. Cheacharoen, and S. Kheawhom, "Linear parameter-varying model for a refuellable zinc–air battery," *Royal Society Open Science*, vol. 7, no. 12, p. 201107, 2020.

[14] A. Abbasi, S. Hosseini, A. Somwangthanaroj, R. Cheacharoen, S. Olaru, and S. Kheawhom, "Discharge profile of a zinc-air flow battery at various electrolyte flow rates and discharge currents," *Scientific data*, vol. 7, no. 1, pp. 1–8, 2020.

[15] Z. Zhao, X. Fan, J. Ding, W. Hu, C. Zhong, and J. Lu, "Challenges in zinc electrodes for alkaline zinc–air batteries: obstacles to commercialization," *ACS Energy Letters*, vol. 4, no. 9, pp. 2259–2270, 2019.

[16] W. Lao-Atiman, P. Bumroongsri, A. Arpornwichanop, S. Olaru, and S. Kheawhom, "Prediction of charge-discharge behavior and state of charge estimation for tri-electrode rechargeable zinc-air flow batteries," *Journal of Energy Storage*, vol. 55, p. 105786, 2022.

[17] J. D. Pineda Rodriguez, S. Olaru, C. Vlad, P. Rodriguez-Ayerbe, W. Lao-Atiman, and S. Kheawhom, "Model-based Voltage Prediction for a Zinc-Air Cell subject to Piecewise Constant Discharge Currents," in *9th International Conference on Control, Decision and Information Technologies, CoDIT 2023*, Rome, Italy, Jul. 2023. [Online]. Available: https://hal.science/hal-04133671